# Slow magnetic relaxation in a homo dinuclear Dy(III) complex in a pentagonal bipyramidal geometry

Joydev Acharya, Naushad Ahmed, J González, Pawan Kumar, Olivier Cador, Saurabh Kumar Singh, Fabrice Pointillart, Vadapalli Chandrasekhar

# Slow Magnetic Relaxation in a Homo Dinuclear Dy(III) Complex in a Pentagonal Bipyramidal Geometry

*Joydev Acharya,[a] Naushad Ahmed,[#b] Jessica Flores Gonzalez,[#c] Pawan Kumar,[a] Olivier Cador,[c] Saurabh Kumar Singh,\*[d] Fabrice Pointillart,\*[c] Vadapalli Chandrasekhar\*[a,b]*

[a]Department of Chemistry, Indian Institute of Technology Kanpur, Kanpur-208016, India. E-mail: vc@iitk.ac.in.

[b]Tata Institute of Fundamental Research, 36/P, Gopanpally Village, Serilingampally Mandal, Ranga Reddy District, Hyderabad 500107, India.

[c]Univ Rennes, CNRS, ISCR (Institut des Sciences Chimiques de Rennes) - UMR 6226, F-35000 Rennes, France. E-mail: fabrice.pointillart@univ-rennes1.fr

[d]Department of Chemistry, Indian Institute of Technology Hyderabad, Kandi-502285, Sangareddy, Telangana, India. E-mail: sksingh@chy.iith.ac.in

[#] The authors contributed equally to this manuscript.

**Abstract**

We hereby report a dinuclear Dy(III) complex, $[Dy(LH_3)Cl_2]_2 \cdot 2Et_2O$ (**1**) (LH$_4$ = 2,3-dihydroxybenzylidene)-2-(hydroxyimino)propanehydrazide) where both the metal centres are in a pentagonal bipyramidal (PBP) geometry with the axial positions being occupied by negatively charged Cl$^-$ ions. The complex as well as it's 10% diluted analogue (**1$_{10}$**) do not show zero-field SMM behaviour. However, in the presence of small optimum *dc* fields the slow relaxation of magnetization was displayed. The effective energy barrier for **1$_{10}$** at 800 Oe of applied field was extracted as 83(17) K with $\tau_0$= 2(4)×10$^{-12}$ s. Through a combined experimental and *ab initio* electronic structure calculations studies we have thoroughly analysed the role of the ligand field around the Dy(III), present in pentagonal bipyramidal geometry, in contributing to the slow relaxation of magnetization.

**Introduction**

The discovery that $[Mn_{12}O_{12}(CH_3COO)_{16}(H_2O)_4]$ displayed single-molecule magnet (SMM) behaviour[1] kicked off intense activity in this area in a truly interdisciplinary manner with the participation of researchers of various backgrounds encompassing experimental and theoretical aspects of chemistry, physics and materials science.[2] Although the initial interest was primarily focused on polynuclear transition metal complexes,[3-6] it soon spread to heterometallic polynuclear 3d/4f complexes[7-9] as well as polynuclear complexes containing lanthanide ions.[10-12] More recently, there has also been interest in coordination complexes containing 4d/5d metal ions[13-21] as well as those that contain actinide metal ions[22-28]. SMMs possess a distinctive bistable ground state and upon magnetization one of these states is populated exclusively. The barrier of magnetization reversal for polynuclear transition metal complexes, $U_{eff}$, depends on both the ground state spin, $S$ and the zero-field splitting parameter $D$ ($U_{eff} = |D|S^2$ when $S$ is even and $|D|(S^2 - \frac{1}{4})$ when $S$ is odd) with the caveat that many relaxation mechanisms exist, including quantum tunnelling of magnetization, that can

undercut the barrier. While the initial efforts were focused on maximizing the ground state spin $S$, the realization that a linear increase of $S$ does not lead to a corresponding increase in $D$,[29] led the re-alignment of the focus of design and assembly to simpler systems containing a fewer number of metal ions with the extreme limit being one.[30] The latter are referred to as mononuclear single-molecule magnets (MSMMs) or single-ion magnets (SIMs). In these cases, the emphasis was on achieving a large magnetic anisotropy while retaining a reasonably high value of ground state spin. Many lanthanide ions such as Dy(III), Tb(III) or Er(III) possessing an intrinsic unquenched spin-orbital angular momentum became the natural targets for designing SMMs/SIMs. Among these metal ions Dy(III) is a Kramers ion and therefore possesses an additional advantage of always possessing a bistable ground state. It is not surprising therefore that the complexes possessing the highest values of blocking temperature (temperatures below which the magnetization is retained/blocked) happen to involve lanthanide metal ions: $[(Cp^{iPr5})Dy(Cp^*)]^+$ where $Cp^{iPr5}$ is penta-iso-propylcyclopentadienyl; $Cp^*$is pentamethylcyclopentadienyl (80 K);[31] $[(Cp^{ttt})_2Dy]^+$ where $Cp^{ttt}$=1,2,4-tri(tert-butyl)cyclopentadienide (60 K)[32, 33]. Long and co-workers have suggested a qualitative prescription of maximizing the single-ion anisotropy of lanthanide ions in a molecular complex by arguing that oblate shaped lanthanide ions like Dy(III), Tb(III), Nd(III) would require a strong axial crystal field to maximize magnetic anisotropy while prolate ions such as Er(III), Yb(III) or Sm(III) would require equatorial fields.[34] The influence of coordination number and geometry in SIMs was assessed by Ungur $et$ $al.$ by theoretical calculations on the hypothetical $[DyF_n]^{3-n}$ complexes.[35] These studies revealed that two-coordinate $[DyF_2]^-$ species having a linear geometry had the highest splitting of the crystal-field (CF) doublets of the ground state $m_J = {}^{15}/_2$ manifold leading to a very high $U_{eff}$ value of around 1800 cm$^{-1}$. Similarly, in an earlier study performed by Chilton the requirement of axial ligand field for high temperature SMMs had also been estimated.[36] However, from a

synthetic point of view, such complexes are elusive. Instead, pseudo linear coordination geometry like pentagonal bipyramid (PBP) possessing a very strong axial crystal field and somewhat weak equatorial field, could be prepared and their properties be assessed.[37] Examples of such mononuclear complexes including [Dy(bbpen)Br](H$_2$bbpen=N,N′-bis(2-hydroxybenzyl)-N,N′-bis(2-methylpyridyl)ethylenediamine);[38] [Dy(O$^t$Bu)$_2$(py)$_5$][BPh$_4$];[39] [L$_2$Dy(H$_2$O)$_5$][I]$_3$ (L= ($^t$BuPO(NH$^i$Pr)$_2$)][40] and dinuclear complexes such as [{Ln(Cp*)$_2$($\mu$-Me$_3$AlNEt$_3$)}$_2$][Al{OC(CF$_3$)$_3$}$_4$]$_2$;[41] [Dy$_2$L$_2$($\mu$-Cl)$_2$(thf)$_2$] (LH$_2$=(N-(2-pyridylmethyl)-N,N-bis(2'-hydroxy-3',5'-di-tertbutylbenzyl)amine));[42] [{Dy($\eta^5$-Cp*)}$_2$($\mu$-BH$_4$){$\eta^5$:$\eta^5$- (1,1′,3,3′-(C$_5$$^t$Bu$_2$H$_2$)$_2$)}]$^+$ [43] or a series of (Co$_2$$^{III}$Dy$_2$$^{III}$) systems[44-46] vindicate the validity of the above argument. In this pursuit, we report, a dinuclear Dy(III) complex, [Dy(LH$_3$)Cl$_2$]$_2$·2Et$_2$O (**1**) where not only both the metal centers possess PBP geometry with a quasi $D_{5h}$ symmetry but where the axial positions are occupied by negatively charged chloride ligands.

**Experimental Section**

Solvents used in this work were purified according to standard procedures.[47] DyCl$_3$·6H$_2$O, 2,3-Dihydroxybenzaldehyde were obtained from Sigma Aldrich Chemical Co. and were used as received. Hydrazine hydrate (80%), ethyl pyruvate, hydroxylamine hydrochloride, sodium acetate, and sodium sulfate (anhydrous) were obtained from S.D. Fine Chemicals, Mumbai, India and were used as such.

**Instrumentation**

Melting points were measured using a JSGW melting point apparatus and are uncorrected. IR spectra were recorded as KBr pellets on a Bruker Vector 22 FT IR spectrophotometer operating between 400–4000 cm$^{-1}$. $^1$H NMR spectra were recorded on a JEOL JNM LAMBDA 400 model spectrometer operating at 500 MHz. Chemical shifts are reported in parts per million (ppm) and are referenced with respect to internal tetramethylsilane ($^1$H).

Elemental analyses of the compounds were obtained from Thermoquest CE instruments CHNS-O, EA/110 model. Electrospray ionization mass spectrometry (ESI-MS) spectra were recorded on a Micromass Quattro II triple quadrupole mass spectrometer. Methanol was used as the solvent for the electrospray ionization.

The SCXRD data for the complexes have been collected on a Bruker SMART CCD diffractometer (MoKα radiation, λ = 0.71073 Å). Collecting frames of data, indexing reflections, and determining lattice parameters was done by the program SMART, integrating the intensity of reflections and scaling was done by SAINT, SADABS[48] for absorption correction, and SHELXTL[49] for space group and structure determination and least-squares refinements on $F^2$. The crystal structures were solved and refined by full-matrix least-squares methods against $F^2$ by using the program SHELXL-2014[50] using Olex-2 software[51]. All other non-hydrogen atoms were refined with anisotropic displacement parameters. The position of the hydrogen atoms was fixed at calculated positions and refined isotropically thoroughly. The crystallographic figures have been generated using Diamond 3.1e program.[52] The crystal data and the cell parameters for the complexes are summarized in Table S1. Crystallographic data (excluding structure factors) for the structures have been deposited with the Cambridge Crystallographic Data Centre (CCDC no 2004909-2004910). Copies of the data can be obtained, free of charge, on application to CCDC, 12 Union Road, Cambridge CB2 1EZ, U.K.: http://www.ccdc.cam.ac.uk/cgi-bin/catreq.cgi, e-mail: data_request@ccdc.cam.ac.uk, or fax: +44 1223 336033.

The *dc* magnetic susceptibility measurements were performed on solid polycrystalline samples with a Quantum Design MPMS-XL SQUID magnetometer between 2 and 300 K in applied magnetic field of 200 Oe for temperatures between 2-20 K, 2 kOe between 20 and 80 K and 10 kOe above. The sample was immobilized in a pellet made with Teflon tape. These measurements were all corrected for the diamagnetic contribution as calculated with Pascal's

constants. The *ac* magnetic susceptibility measurements were performed on Quantum Design MPMS-XL SQUID magnetometer in the frequency range of 1 to 1000 Hz.

**Computational Details**

All the calculations were performed on the X-ray crystal structure, where the positions of hydrogens were optimized with ORCA code [53, 54] using BP86 functional and def2-SVP type basis set (see ESI for optimized coordinates). All the quantum chemical calculations were performed using MOLCAS 8.2.[55] The spin-Hamiltonian parameters were calculated by using a complete active space self-consistent field (CASSCF) method. We have employed the [ANO-RCC…8s7p5d3f2g1h] basis set for Dy and Lu atoms, the [ANO-RCC…4s3p1d] basis set for Cl atom, the [ANO-RCC… 3s2p1d] basis set for O and N atoms, the [ANO-RCC…3s2p] for the rest C, and the [ANO-RCC…2s] basis set for H atoms.[56, 57] For calculations of single-ion properties of Dy(III) ion in complex **1**, we have replaced one of the two Dy(III) ions by the diamagnetic Lu(III) ion in the crystal structure. The electronic configuration of the Dy(III) ion is $4f^9$, possessing $^6H_{15/2}$ ground state. The active space comprised of CAS(9,7), *i.e.*, all the nine active f-electron in the seven active f-orbitals, was used for calculation of magnetic properties. Using this active space, we have computed 21 spin-free sextet states and 224 quartet states, and subsequently, we mixed 21-spin-free sextet and 108 quartet states below ~ 40000 cm$^{-1}$ in the spin-orbit restricted active space state interaction (SO-RASSI) module [58] to compute the spin-orbit states. We have also computed SOC states using only 21 spin-free sextet states. These computed spin-orbit states were then used to compute the *g*-values, crystal field parameters, and transition magnetic moment matrix for individual Dy(III) ions using the SINGLE_ANISO module as implemented in the MOLCAS 8.2 code.[59] The Cholesky decomposition for two-electron integrals was employed throughout the calculations to save the disk space. The exchange spectrum (dipolar and exchange contributions), along with the magnetic properties of the dinuclear compound, was

simulated using POLY_ANISO code based on obtained results from the *ab initio* calculations. The POLY_ANISO code has been successfully used to simulate the magnetic properties of highly anisotropic polynuclear complexes. [60,61, 62-64]

To compute the isotropic part of the exchange interaction, broken-symmetry density functional theory (BS-DFT) calculations with B3LYP exchange-correlation functional were performed in ORCA 4.2.1 code.[53, 54] Dispersion corrections were treated by Grimme's atom-pairwise dispersion correction approach. Calculations were performed on the isotropic Gd(III)-Gd(III) dinuclear complex, and the $J$ values were further scaled for Dy(III) by a factor 49/25 as mentioned earlier.[65, 66] Scalar relativistic effects were incorporated through Douglas-Kroll-Hess (DKH) approximation.[67] Here, we have used all-electron scalar relativistic (SARC) basis set for Gd,[68] in combination with DKH reconstructed versions of def2 –type basis sets; DKH-def2-TZVP for Cl and DKH-def2-SVP for the rest of the atoms as implemented in ORCA code. Resolution of identity chain-of-spheres (RIJCOSX) approximation, increased grid settings (GRIDX9 for Gd and GRIDX6 for rest of the atoms) along with corresponding auxiliary basis sets were used to speed up the calculations. The exchange coupling was computed with the Yamaguchi formula[69] by scaling the energy difference between the high-spin and broken-symmetry solutions according to their spin expectation values.

**Synthesis**

The ligand $LH_4$ is synthesised according to our previously reported procedure.[70]

**Synthesis of $[Dy(LH_3)Cl_2]_2 \cdot 2Et_2O$ (1)**

To a 30 mL ethanolic solution of 0.048 g $LH_4$ (0.2 mmol) in a 100 mL round bottom flask was added 0.075 g (0.2 mmol) of $DyCl_3 \cdot 6H_2O$ and stirred at room temperature for 2h followed by complete evaporation of the solvent in vacuo. The obtained semisolid was washed thoroughly with diethyl ether followed by drying and re-dissolving in 2-3 mL of

ethanol. Yellow crystals were obtained by slow diffusion of diethyl ether into the ethanol solution of the compound at room temperature. Yield: 0.099 g (46%, on the basis of Dy(III) salt). Anal. Calcd. For $C_{28}H_{40}Cl_4Dy_2N_6O_{10}$ (1087.46):C, 30.93; H, 3.71; N, 7.73; found: C, 30.94, H, 3.46, N, 7.69.

**Synthesis of $[Y(LH_3)Cl_2]_2 \cdot 2Et_2O \cdot H_2O$ ($1_Y$)**

A similar synthetic procedure was adapted as for **1**, but $YCl_3 \cdot 6H_2O$ (0.061 g) was used instead of $DyCl_3 \cdot 6H_2O$. Yield: 0.131 g (68%, on the basis of Y(III) salt). Anal. Calcd. For $C_{28}H_{42}Cl_4N_6O_{11}Y_2$ (958.29):C, 35.09; H, 4.42; N, 8.77; found: C, 35.23, H, 4.62, N, 8.85.

The Single crystal XRD measurement was done on $1_Y$. The unit cell measurement revealed that $1_Y$ has an almost similar unit cell parameter and packing pattern like in **1** (see Table S1). Therefore, it was used as a diamagnetic matrix to host the corresponding paramagnetic Dy(III) analogue.

**Preparation of 10 % diluted sample of 1 ($1_{10}$)**

A similar synthetic procedure was adapted as for **1**, but instead of only Dy (III) salt both $DyCl_3 \cdot 6H_2O$ (0.0075 g, 0.02 mmol) and $YCl_3 \cdot 6H_2O$ (0.055g, 0.18 mmol) were added at the same time. Powder X-ray diffraction measurement for $1_{10}$ was done and found that the sequence and pattern of the peaks are sufficiently in good agreement with the simulated data obtained from PXRD data of the corresponding Dy(III) analogue (see Figure S1).

**Results and Discussion**

**Synthetic Aspects**

Aroylhydrazone-based Schiff base ligands have been shown to be very useful for synthesizing homometallic lanthanide(III) complexes of varied nuclearity.[70-74] These ligands possess interesting features like the possibility of having keto or enol form or both, depending on the coordination requirements and also the possibility of having C-C/ N-N bond rotation which lends additional flexibility to the ligand. We had previously utilized these features in

the formation of $Dy_2$, $Dy_4$, $Dy_6$, and $Dy_{21}$ complexes by using an aroylhydrazone-based Schiff base ligand, 6-((bis(2-hydroxyethyl)amino)methyl)-$N'$-((8-hydroxyquinolin-2-yl)methylene)picolinohydrazide ($L'H_4$) ligand.[74] We had also used, the ligand of interest in the current study, $LH_4$, along with additional ancillary $\beta$-diketonate co-ligands for the synthesis of a series of linear $Dy_4$ complexes[70] (Scheme 1). Inspired from these results, it was of interest to examine the fate of the reaction of $LH_4$ with Dy(III) salts without using any chelating counter anion (like $OAc^-$, $NO_3^-$) or any co-ligand or a base.
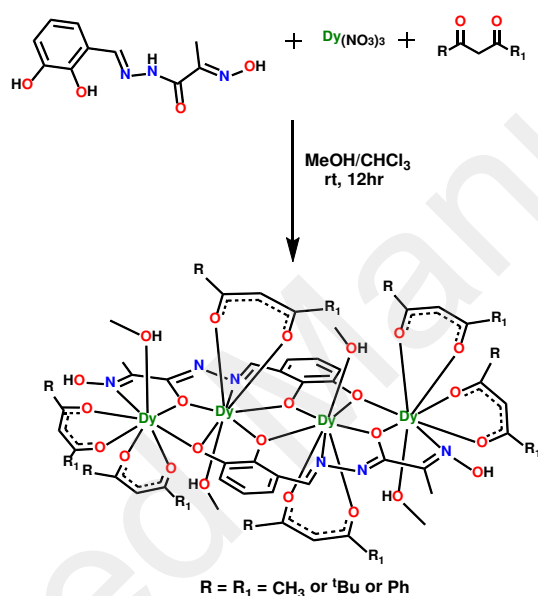


**Scheme 1**. The synthesis of the linear $Dy_4$ complexes by using the ligand, $LH_4$.[72]

Accordingly, the reaction of $LH_4$ with $DyCl_3 \cdot 6H_2O$ in a molar ratio of 1:1 afforded a dinuclear complex of formula $[Dy(LH_3)Cl_2]_2 \cdot 2Et_2O$. Interestingly, both the Dy(III) centers in this complex have been shown to possess a pseudo $D_{5h}$ geometry (Scheme 2; see below for description of the molecular structure).

In order to check the stability of the complex in the solution we carried out ESI-MS studies which revealed a complete fragmentation of the complex under the experimental conditions (Figure S2).
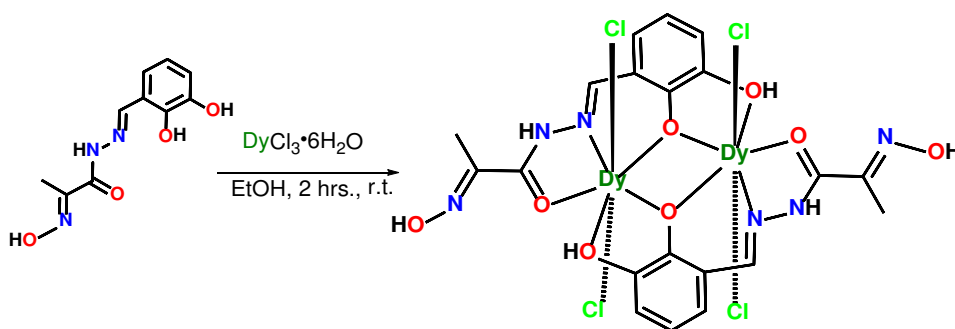
**Scheme 2**. Synthesis of complex **1**.

### X-ray crystallography

Single crystal studies revealed that **1** crystallized in the monoclinic *C*2/c (N°15) space group as a charge-neutral metal complex. The asymmetric unit of the complex contains one-half of the entire molecule (Figure 1), and the full molecule is generated because of a center of inversion present in the complex.
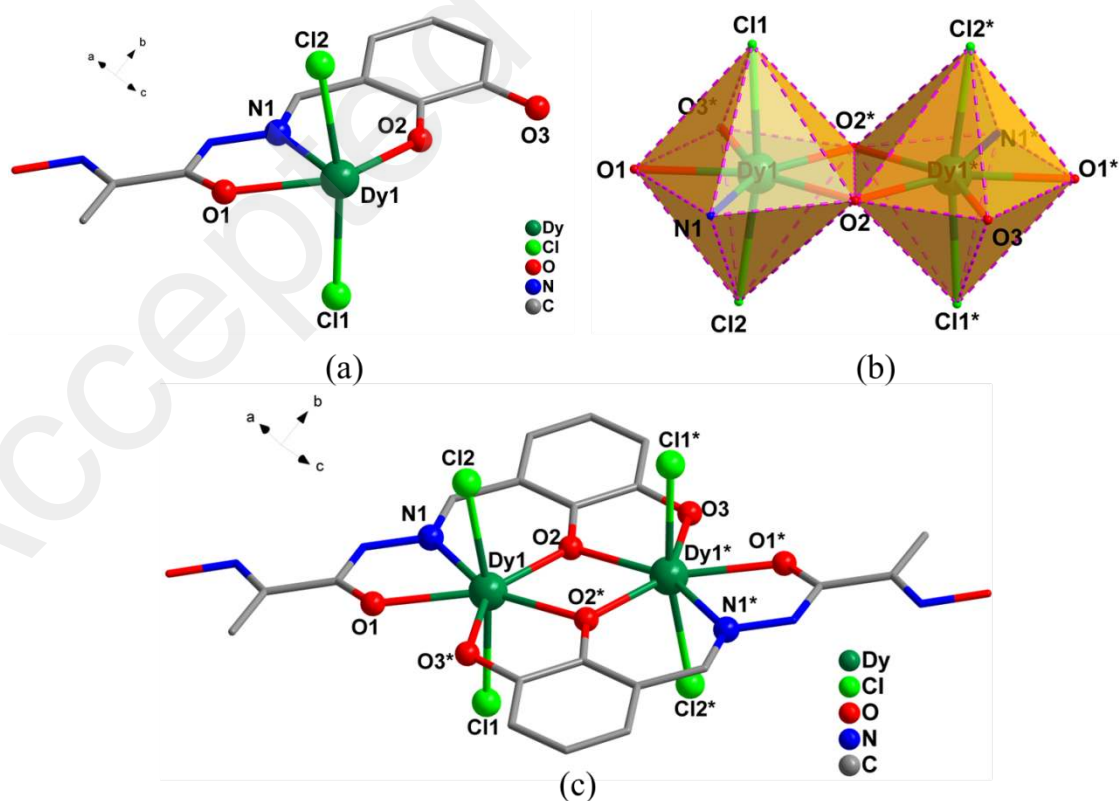


(a)

(b)

(c)

**Figure 1**. a) The asymmetric unit of **1**, b) pentagonal bi-pyramidal geometry around both the Dy(III) centers in **1**, c) full molecular structure of **1**. (All the hydrogen atoms and solvent molecules are omitted for the sake of clarity. Atoms labelled with asterisks belong to the other half of the asymmetric unit).

As the molecule possesses a centre of symmetry all the bond parameters concerned to one metal (Dy1) centre will be exactly similar to the other metal centre (Dy1*). Selected bond parameters around Dy1 are given in Table S3. Complex **1** is assembled by the involvement of two mono deprotonated ligands (only the phenol motif of the ligand is de-protonated). The two phenolate units arising from the two ligands assist in bridging the two Dy(III) centers and in forming the resulting [$Dy_2O_2$] four-membered ring. Each ligand potentially has three types of coordination pockets as shown in Figure 2. Out of these, pocket 3 remains completely unused, leaving the oxime-motif free. The formation of the dinuclear complex is related to the single de-protonation. If all the potential protic sites were de-protonated, proliferation of the metal assembly would have been the result.
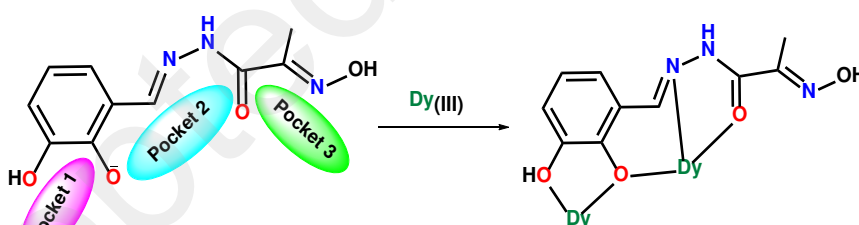


**Figure 2**. Three coordination pockets of [$LH_3$]$^-$ and its binding mode ($\mu^2$-$\eta^1$:$\eta^2$:$\eta^1$: $\eta^1$).

Four Dy-O bonds are present around each Dy(III) center. All the bond distances appear to be similar (Table S3). The only Dy-N bond present is seen to be longer (2.4595(6) Å) than the all four Dy-O bonds. In order to find the exact geometry and magnitude of distortion around the metal centers we carried out continuous SHAPE measurement[75, 76] and have found that

both the Dy(III) centers are in an approximately pentagonal bipyramidal (PBP) geometry with a minimum amount of distortion (Table S2). In the PBP geometry the equatorial positions are occupied by four oxygens and one nitrogen atoms while the apical positions contain two chloride ions with the Cl1-Dy1-Cl2 bond angle (169.779(6)°) indicating a slight distortion from the ideal 180°. The Dy1-Cl1 and Dy1-Cl2 bond lengths are 2.6114(2) and 2.6266(2) Å respectively.

Although there are a few examples of mononuclear Dy(III) complexes in PBP geometry and having both the axial coordination by Cl⁻ ions, the dinuclear complex described here where both the metal ions are in PBP geometry with axial chlorides represents a rare example. [77, 78] In addition to **1** there are only three more such examples (Figure 3). Table 1 contains a comparison of the bond parameters and the magnetic data of **1** with related examples.



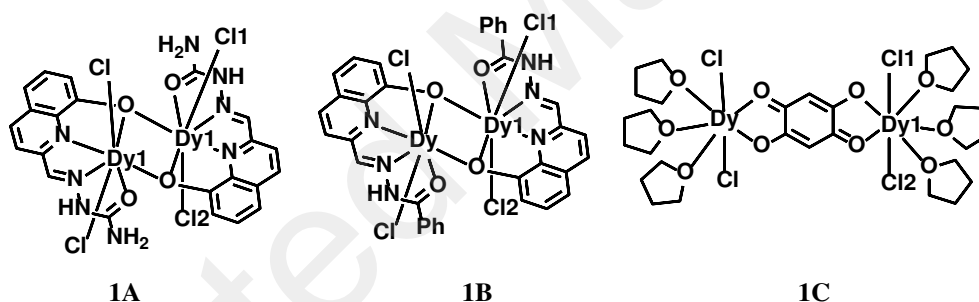**1A**          **1B**          **1C**

**Figure 3.** Molecular structures of the literature reports of the Dy$_2$ complexes in PBP geometry. [77, 78] (A few atoms are labelled in the figures for the clarification of the bond parameters shown in Table 1).

**Table 1**. A comparison of selected bond lengths (Å) and bond angles (°) of complex **1** with some other literature reported Dy₂ complexes in PBP geometry.

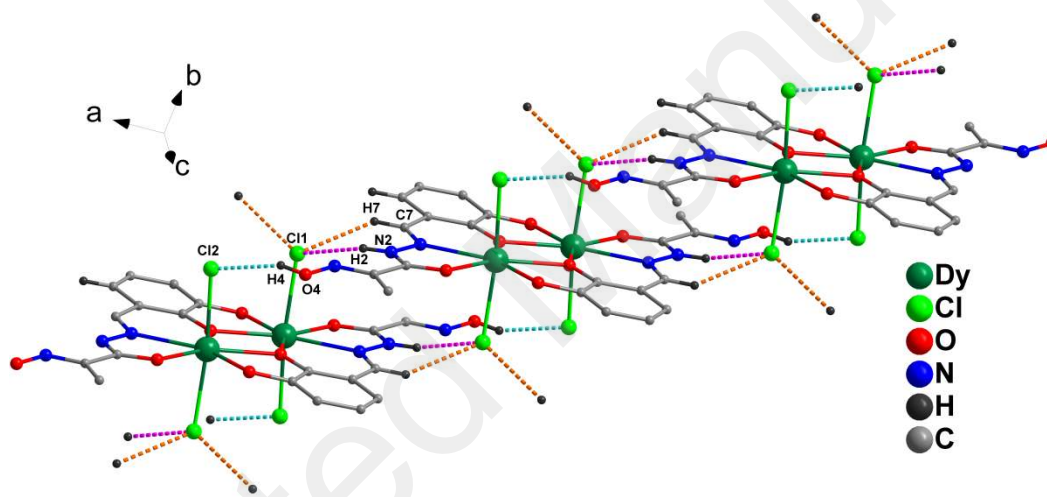| Com plex | Axial Bonds Lengths (Å) | | Axial Bond Angle (°) | Δ in K and $\tau_0$ (s) | $H_{dc}$ (Oe) | Ref. |
|---|---|---|---|---|---|---|
| | Dy1—Cl2 | Dy1—Cl1 | Cl1-Dy-Cl2 | | | |
| **1** | 2.626(2) | 2.611(2) | 169.78(6) | 83(2) and $\tau_0$= $2(4) \times 10^{-12}$ | 800 | This work |
| **1A** | 2.629(2) | 2.599(2) | 165.84(7) | 83.64 and $\tau_0$ = $8.62 \times 10^{-10}$ | 900 | [77] |
| **1B** | 2.609(1) | 2.591(1) | 163.30(4) | 101.43 and $\tau_0$ = $9.92 \times 10^{-11}$ | 900 | [77] |
| **1C** | 2.587(2) | 2.603(2) | 175.87(8) | - | - | [78] |



**Figure 4**. Intermolecular hydrogen bonding mediated 1D supramolecular structure of **1**. Selected hydrogen atoms and solvent molecules omitted for clarity.

The supramolecular assembly of **1** is mediated by three kinds of non-covalent interactions: C–H···Cl; N–H···Cl; O–H···Cl (Figure 4). Of these, O–H···Cl is an intramolecular interaction and is found between the OH group of the oxime part of the ligand and the coordinated Cl⁻ ion (O4–H4···Cl2 [2.337(2) Å]). The other two *viz*., C–H···Cl and N–H···Cl interactions are intermolecular and are quite strong (C7–H7···Cl1 [2.658(2) Å]; N2–H2···Cl1

[2.409(2) Å]). These interactions result in a 1D chain. Such chains grow into 2D sheets via inter-chain interactions involving aromatic C–H and the coordinated Cl$^-$ ion (C5–H5···Cl1 [2.831(2) Å]) (Figure 5).
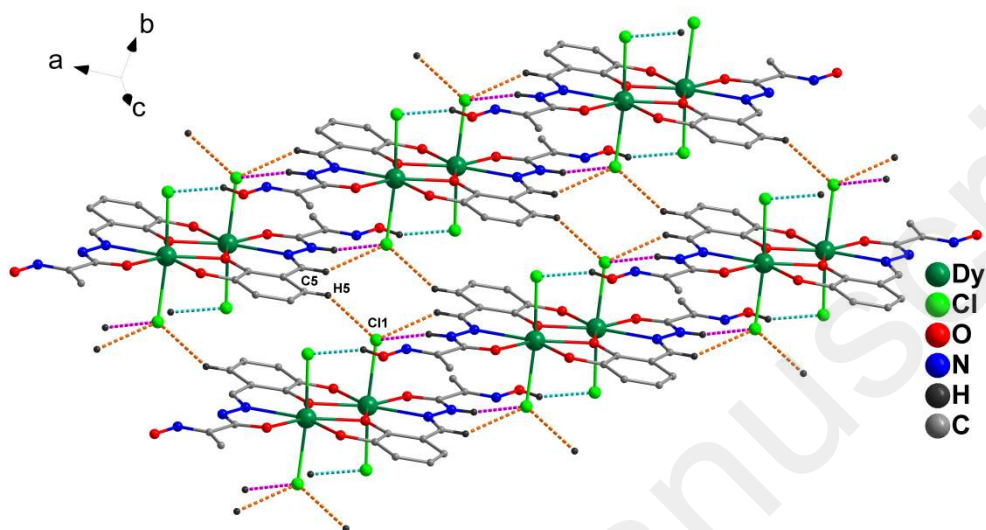


**Figure 5**. Formation of a 2D sheet via inter-chain C–H···Cl interaction.

**Magnetic Properties**

*Dc* magnetic properties were determined by measuring the thermal dependence of the molar magnetic susceptibility ($\chi_M$) from 2 to 300 K for both **1** (Figure 6) and **1$_{10}$** (Figure S3). For **1**, at room temperature the $\chi_M T$ *vs.* T curve reaches 27.88 cm$^3$ K mol$^{-1}$, close to the expected value of 28.4 cm$^3$ K mol$^{-1}$ for two isolated Dy(III) ions ($^6H_{15/2}$ and $g_J$=4/3).[79] On cooling, $\chi_M T$ remains constant down to 100 K and then decreases progressively reaching a minimum of 14.13 cm$^3$ K mol$^{-1}$ at 2 K. This decrease can be mainly attributed to the depopulation of the ligand-field levels, which is accentuated at the lower temperatures due to the existence of weak antiferromagnetic interactions. At 2K, the field dependence of the magnetization shows a classic behaviour with a value of 10.89 Nβ at 50 KOe for two trivalent dysprosium ions, which is in agreement with the presence of an *Ising* ground state. On the other hand, the magnetism of **1$_{10}$** is estimated to represent only 5% of the magnetization, in opposition with

the expected 10 % used during the synthetic protocol. Such discrepancy could be explained by a greater affinity for the Y(III) than for Dy(III) as attested by the higher yield for the synthesis of **1$_Y$** (64 %) than for **1** (49 %).
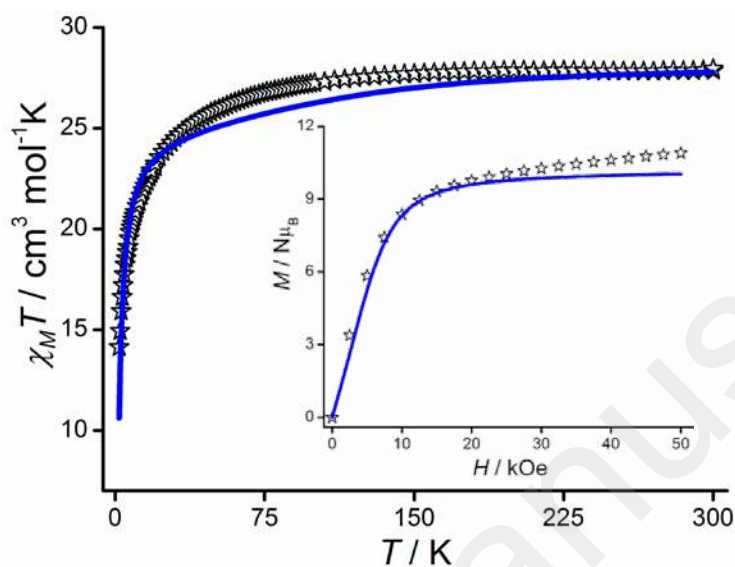


**Figure 6**. Thermal dependence of the $\chi_M T$ product for **1** (open symbols). The inset corresponds to the field dependence of the magnetization at 2 K. Blue lines correspond to the best simulated curves from POLY_ANISO program implemented in MOLCAS 8.2 package.

Dynamic magnetic measurements (*ac*) have been performed for **1** and **1$_{10}$**. At zero *dc* magnetic field the samples displayed no or very weak out-of-phase component of the susceptibility at 2 K in the window 1-1000 Hz frequency of the oscillating field (Figure S4 and S5). The application of a *dc* magnetic field induces a frequency dependence on the out-of-phase susceptibility ($\chi_M''$) and the suppression of a possible QTM regime.[80-82] Applying an external *dc* magnetic field, an out-of-phase contribution of the magnetic susceptibility appeared at 270 Hz. Increasing the value of the *dc* field, $\chi_M''$ remains centered at the same frequency but its intensity increased until 2000 Oe (Figure S4). Nevertheless, for a magnetic field value higher than 1200 Oe a shoulder appears at a lower frequency. Thus, a compromise for the suitable value of the applied field is 1200 Oe for the condensed sample (Figure S4).

For the diluted analogue, the slowest relaxation is observed at an optimal *dc* magnetic field of 800 Oe (Figure S5). Figure 7 shows the frequency dependence of $\chi_M''$ for **1** (Figure 7a) and **1$_{10}$** (Figure 7b) between 2 and 8 K at the optimal field. At 2 K, $\chi_M''$ *vs.* $\nu$ curve passes through a maximum at 270 Hz, for **1**, which is shifted to 17 Hz upon dilution (**1$_{10}$**). At this point it is worth notice that we observed a slight deviation for the magnetic susceptibility intensities between the field and thermal dependences measurements.
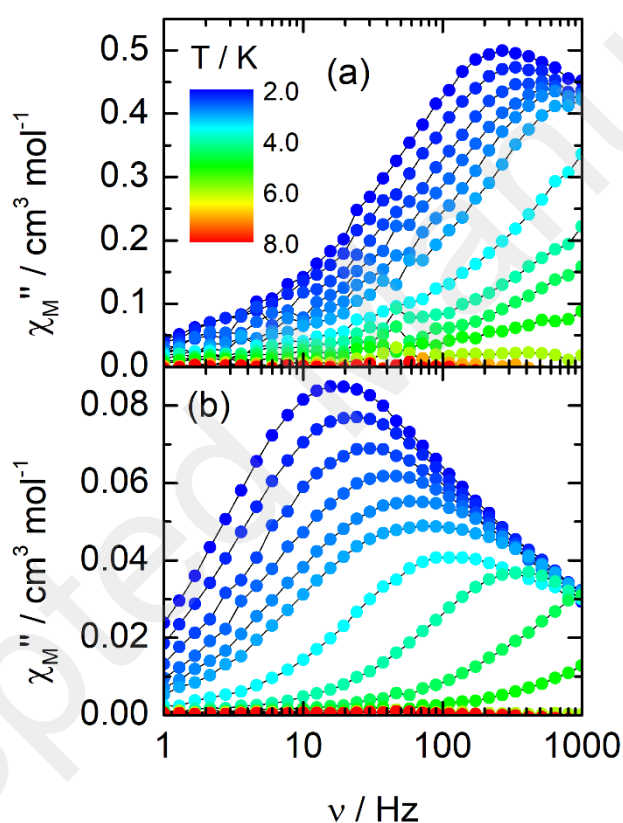


**Figure 7**. a) Out-of-phase component of the *ac* magnetic susceptibility data for **1** and b) **1$_{10}$** between 2 and 8 K under 1200 and 800 Oe applied fields respectively.

The relaxation time ($\tau$) for both systems has been extracted with an extended Debye model[83, 84] (see SI, Figures S6-S10, Tables S4-S5). Further information is given by the $\alpha$ parameter

and the ratio between the isothermal and adiabatic susceptibilities ($\chi_T$ and $\chi_S$) as follows:
$\chi_T - \chi_S / \chi_T$. Indeed, there is a small fraction of **1** displaying slow relaxation of the magnetization (around 30%) and within a quite large distribution of the relaxation times (0.36<$\alpha$<0.39) (Table S4). By dilution of the system (Table S5), and the consequent decreasing of the interactions, the slow relaxation of the magnetization is enhanced achieving a fraction close to 85% of the sample, and a slightly smaller distribution (0.17<$\alpha$<0.41). In Figure 8, the dependence of $\tau$ with temperature is represented. As appears, the experimental information obtained for **1** is not sufficient to obtain a good characterization of the dynamics of the system, mainly concerning the Orbach process, making necessary a first determination by the results obtained for **1$_{10}$**.
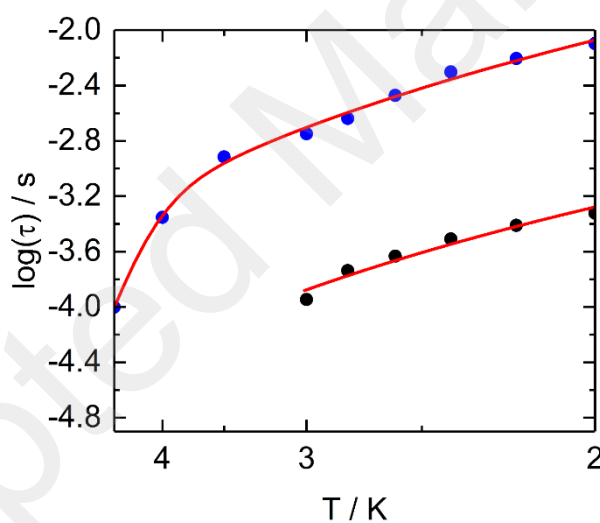


**Figure 8**. Arrhenius plots of the relaxation times in 800 Oe for **1$_{10}$** (blue disks) and 1200 Oe for **1** (black disks). Full lines are the best-fitted curves (see text).

The thermal dependence of $\tau$ for **1$_{10}$** follows a modified Arrhenius law. The difference in the slope of the $\tau$ *vs.* $T^{-1}$ curve makes us consider the important effect of the Raman process, which is supported by the small effective barrier compared to the calculated values (344 K and 347 K, see computational part). It is worth noting that the Orbach only fitting of the high

temperature region gave an energy barrier value of about 54 K. The best fit has been obtained, considering both thermally dependent Orbach and Raman processes (equation 1). In the following equation the first term of the equation represents the Orbach and the second term, the Raman process:[85]

$$\tau^{-1} = \tau_0^{-1} \exp\left(\frac{-\Delta}{T}\right) + CT^n$$ ----------------------- Equation 1

with $\Delta = 83(17)$ K, $\tau_0 = 2(4) \times 10^{-12}$ s, $C = 10(2)$ s$^{-1}$K$^{-n}$ and n=3.6(3). The expected n value for Kramers ions should be 9,[86] but the presence of both acoustic and optical phonons could lead to lower values comprised between 2 and 7.[87, 88] At the same time, dilution is well known not to modify the field independent Orbach regime.[89] So far, if we compare both systems, in **1** this regime is clearly not achieved within the temperature range. With the attempt to find a more accurate description of the relaxation mechanism in **1**, the fitted Orbach parameters for **1$_{10}$** have been maintained constant and used for fitting the Arrhenius plot of **1**. The best fitted parameters resulted in an increase of the C constant up to 180(58) s$^{-1}$ K$^{-n}$ with a nearly unchanged temperature dependence of n = 3.4(4). This modification of the Raman process could be explained given the fact that the matrix is modified with the exchange of Dy(III) (in **1**) with Y(III) (in **1$_{10}$**).[90]

**Computational Studies**

To gain insight into the electronic structure and to confirm the observed *dc* magnetic properties, *ab initio* based CASSCF calculations were performed on complex **1**. This CASSCF based approach has been widely used to analyse the electronic and magnetic properties in a variety of highly anisotropic lanthanide/actinide complexes. [40, 59, 91-98] The details of the methodology are provided in the computational details section. First, we have focussed on understanding the local electronic structure of the Dy(III) ion, and here we have computed single-ion anisotropy of individual Dy(III) ions by replacing one of the Dy(III) ion

by its diamagnetic analogue Lu(III) . Here, we have computed 21 sextets and 224 quartet spin-free states with CAS (9,7) active space. The spin-free sextet states spanned over an energy window of ~35160 cm$^{-1}$ with the first excited state being ~6.3 cm$^{-1}$ above the ground state for both the Dy1 and Dy2 centres in complex **1**. By contrast, the spin-free quartet states spanned an energy window of 24876-106935 cm$^{-1}$ for both the Dy1 and Dy2 centres in complex **1.** Due to the centre of symmetry, the energy manifold of spin-free and spin-orbit states is nearly the same. The relative energy of computed spin-free states, spin-orbit states, and the *g*-values are provided in Tables S6-S10. It is evident from Tables S9 and S10 that the low-lying eight Kramers doublet (KD) generated from the $^{6}H_{15/2}$ ground state spans over a range of ~418 cm$^{-1}$ for both Dy1 and Dy2 centres. For individual Dy(III) ions the computed *g*-values are highly axial in nature (($g_{xx}$ = 0.0008, $g_{yy}$ = 0.0021 and $g_{zz}$ = 19.8622) for Dy1; ($g_{xx}$ = 0.0009, $g_{yy}$ = 0.0022 and $g_{zz}$ = 19.8783) for Dy2). Wave function decomposition analysis indicates that the ground state of both Dy(III) ions are predominantly $m_J$ ±15/2 with a small admixing from the other excited states (see Table S11). The computed ground state is highly axial; however, it lacks the pure *Ising* type ($g_{xx}$ = $g_{yy}$ ≈ 0; $g_{zz}$ ≈ 20 ) feature, and this indicates that the possibility of QTM within the ground state KD cannot be completely ruled out. The axiality in the *g*-values of the individual Dy(III) ions are related to the axial crystal field generated by the PBP geometric environment. The computed main magnetic axis of both Dy(III) ions are almost parallel to each other (~ 0.37°) and directed toward axially coordinated Cl$^{-}$ ligands (see Figure 9). The gap between the ground and first excited KD is ~ 239 cm$^{-1}$ for both the Dy1 and Dy2 centres. The first excited KD is predominantly $m_J$ ±13/2 with a significant admixing from the $|±1/2⟩$, $|±5/2⟩$ excited KDs (see Table S11). As a result, significantly large transverse component in the computed *g*-values of first excited KD ($g_{xx}$ = 1.9391, $g_{yy}$ = 2.4122 and $g_{zz}$ = 14.4857 for Dy1 and $g_{xx}$ = 1.8180, $g_{yy}$ = 2.0794 and $g_{zz}$ = 14.7238 for Dy2) is witnessed. The orientation of the $g_{zz}$ axis of the first excited KD is nearly

collinear with ground state KD (~3.2°) from the ground state main anisotropy axis. Due to the presence of such large transverse anisotropy in the first excited KD, it is reasonable to consider that magnetic relaxation is likely to occur via first excited KD.
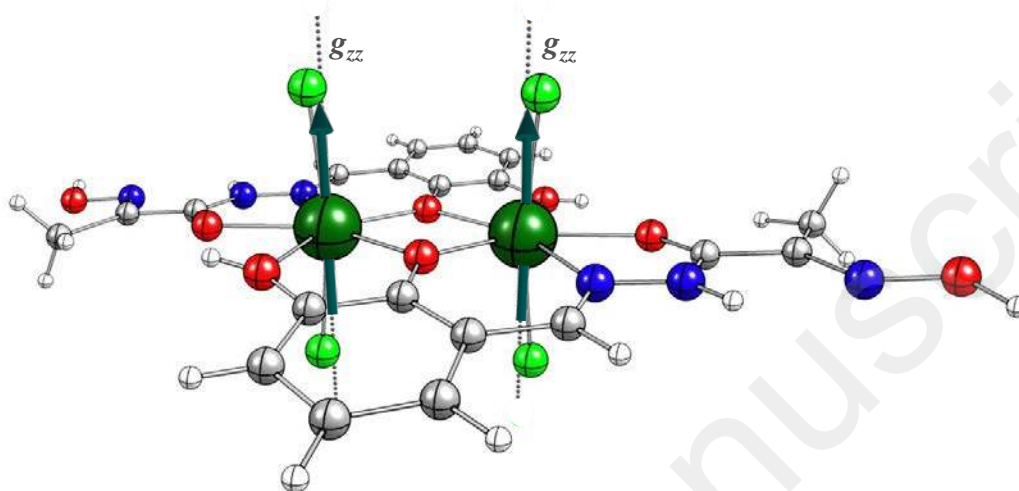


**Figure 9**. *Ab initio* computed orientation of main magnetization axes of individual Dy(III) centres in **1**. Colour code: Green (Dy), blue (N), red (O), grey (C), light green (Cl) and H (white).

To further probe the nature of magnetic relaxation in both the Dy(III) centres, transverse magnetic moments[99] between the KDs were computed (see Figure 10). For ground-state KD the transverse magnetic moment is non-negligible ($0.51 \times 10^{-3}$ $\mu_B$ for Dy1; $0.53 \times 10^{-3}$ $\mu_B$ for Dy2) indicating that QTM within the ground state KD is partially operative ($< 10^{-6}$ criteria for complete quenching).[38, 40, 100] The transverse magnetic moment between the ground and first excited KD is 1.62, which is larger than the value for ground state connecting doublet, suggesting relaxation to occur via the excited KDs. Interestingly, the transverse magnetic moment between the connecting first excited KD is very large (0.72 $\mu_B$ for Dy1 (0.66 $\mu_B$ for Dy2), and this enforces magnetic relaxation via the first excited KD. Thus, most likely, magnetic relaxation is expected to occur via the first excited KD through TA-QTM. The *ab initio* computed barrier height for the individual Dy1 and Dy2 centers are ~239 cm$^{-1}$, and this

is much larger compared to the experimental barrier height of 83 K (~58 cm$^{-1}$). In general, the calculated barrier heights for Dy-based SIMs are quite comparable with the experimentally reported barrier height.[101, 102] However, in this case, the theoretically calculated barrier height is almost four times higher in energy compared to the experimental $\Delta$ value of 83K (~58 cm$^{-1}$) extracted from the equation 1. Such a large discrepancy between the computed and experimental barrier height might be due to the magnetic relaxation through under-energy processes such as Raman relaxation. The presence of intermolecular interaction, which is completely missing in our model calculations, cannot be put aside since they often favour QTM and open up multiple channels for magnetic relaxation, which reduces barrier height. The crystal structure packing of **1** shows very strong intermolecular and interchain interaction, resulting in a very short Dy···Dy distances < 9.5 Å (see Figure 4 and Figure 5).[103-107] As a result, one would expect a strong dipolar interaction to induce the QTM, which would eventually decrease the thermal energy barrier to an effective value. Alongside the presence of other interactions such as hyperfine interactions,[108-110] vibronic coupling,[111, 112] and dynamic nature of electrons[113], too, can play a crucial role in determining the barrier height.
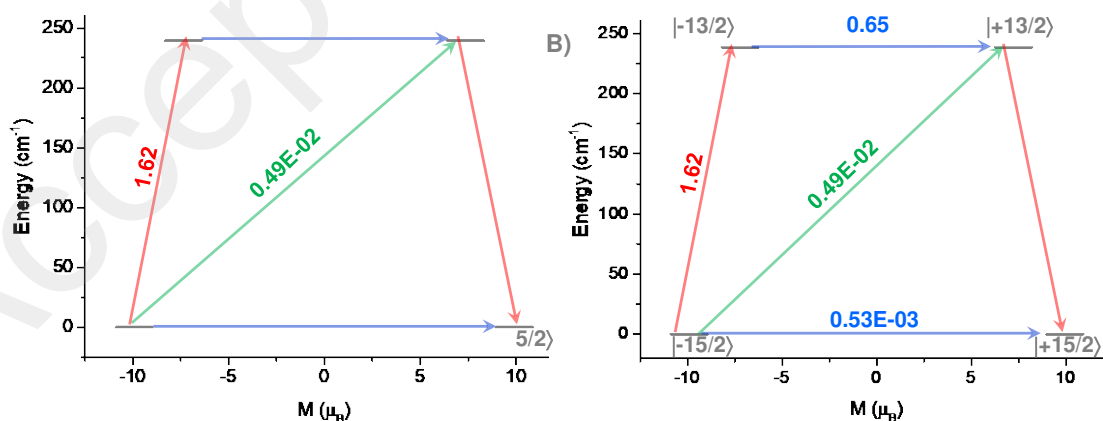


**Figure 10**. a) *Ab initio* computed magnetic relaxation pathway of the Dy1; b) Ab initio computed magnetic relaxation pathway for Dy2 centres in **1**. The grey line indicates the KDs

as a function of magnetic moments. The red, blue and green lines represent thermal, QTM, and possible Orbach relaxations.

It is worth noting that PBP geometry is one of the preferred geometry for accessing the axial ligand field to build highly anisotropic Dy(III) based single-ion magnets.[37] Numerous mononuclear Dy(III)- based SIMs in PBP geometric environment are reported in the literature with the barrier height as high as 1000 K[114] and magnetization blockade up to 20 K.[115] Interestingly, in **1**, both the Dy(III) ions reside in the PBP environment, and our theoretical analysis suggests that these ions lack pure *Ising* type $m_J$ ±15/2 ground state and relax via first excited KD ($U_{cal}$ ~239 cm$^{-1}$ ). To understand the nature of axiality and ligand field interaction, here we have computed the crystal field parameters (CF) as implemented in the MOLCAS 8.2 code. The CF parameters were computed using the following equation, $\widehat{H_{CF}} = \sum \sum_{k=-q}^{q} B_k^q O_k^q$ and here $B_k^q$ and $O_k^q$ are the crystal field parameters and Steven's operator, respectively (see Table S12). The computed axial $B_2^0$ parameter is highly negative and an order of magnitude large compared to the $B_2^{(q=2,4,6)}$ nonaxial parameters, indicating stabilization of the $m_J$ ±15/2 as the ground state. The presence of notable non-axial $B_2^{(q=2,4,6)}$ parameters result in a non-negligible transverse anisotropy in ground state *g*-values of both Dy(III) ions. Moreover, the other higher-order non-axial $B_4^{(q=2,4,6)}$ , $B_6^{(q=2,4,6)}$ terms are much larger compared to the axial $B_4^0, B_6^0$ terms and therefore indicating that Dy(III) ions in the PBP environment do not access the complete axial crystal field. A close inspection of structural parameters suggests that the average Dy-L (L =O/N donor ligands) equatorial bond is ~ 2.357 Å, and this is much shorter compared to average Dy-Cl axial bonds of 2.6185 Å. Thus, from a structural viewpoint, it clear that both the Dy(III) ions are in the axially elongated PBP environment, which is an adverse situation to stabilize the pure $m_J$ ±15/2 as the ground state. To further gain insight into the donor strength of the ligand field, we have

analysed CASSCF computed LoProp charges.[116] The computed LoProp charges show a sizeable negative charge on axially coordinated –Cl atoms compared to other atoms in the equatorial plane (see Table S13). Most importantly, the ratio of the average axial/equatorial LoProp charges and bond lengths are opposite to each other. As a result, both the Dy(III) ions face an intermediate ligand field (an average repulsion from both axial and equatorial ligands), where ligand field stabilized $m_J$ ±15/2 as a ground state at the expense of significant mixing from other excited states. This is visible in the CASSCF computed beta spin-density, which lacks typical oblate type disk shape of $m_J$ ±15/2 ground state of Dy(III) ions (see Figure S11).[117] Thus, in contrast to high-performant Dy-based SIMs in the PBP environment (where axial bonds are short compared to equatorial bonds), short equatorial Dy-L bond and asymmetric CF interactions lead to significant transverse anisotropy and activate the QTM, which eventually diminishes the SMM property of **1**.

**Table 2**. Exchange and dipolar interaction obtained from the best fit using Lines model along with the low-lying exchange spectrum. All the values here are reported in cm$^{-1}$.

| Interaction | Energy | |
|---|---|---|
| $J_{tot}$ | -0.008 | |
| $J_{dipo}$ | 0.142 | |
| $J_{exch}$ | -0.15 | |
| $J_{exch}$(BS-DFT)* | -0.42 | |

| Energy | $\Delta_{tunnel}$ | $g_{zz}$ |
|---|---|---|
| 0.0 0.0 | -3.31E-08 | 0.0194 |
| 1.8 1.8 | 4.71E-08 | 39.7406 |
| 238.9 238.9 | 3.23E-05 | 4.9721 |
| 239.7 239.7 | 3.54E-05 | 4.7229 |
| 240.3 240.3 | 5.27E-05 | 34.3500 |
| 240.3 240.3 | 4.96E-05 | 34.5700 |

* see computational details and Table S14

To compute the exchange spectrum, magnetic properties, and how it affects the magnetic relaxation in **1**, we have used the POLY_ANISO code. In this approach, magnetic susceptibility and magnetization data were fitted using the Lines model to extract the exchange interaction between the Dy(III) centres, while the contribution from intramolecular dipole-dipole interaction is accounted. The magnetic exchange interactions (exchange + dipole) between Dy(III)) centres were modelled by $\hat{H} = -(J_{exch} + J_{dip})S_{1z}S_{2z}$ where $J_{exch}$ and $J_{dip}$ are the exchange and dipolar coupling respectively, while $S_{1z}$ and $S_{2z}$ are the projection of pseudo-spin $S= \frac{1}{2}$ of the ground state KD of Dy1 and Dy2 centres. The best fit of the experimental magnetic susceptibility and magnetization data (see Figure 6) yields the $J_{tol}$ = -0.008 cm$^{-1}$ ($J_{exch}$ = -0.15 cm$^{-1}$ and $J_{dip}$ = 0.142 cm$^{-1}$). Based on the resulting exchange spectrum, all the magnetic properties were computed. The calculated exchange spectrum, tunnel splitting along with *g*-values for **1** is provided in Table 2. From Table 2 it evident that both the exchange and dipolar interactions are of similar strength but opposite in sign. To further probe the sign of exchange interaction, scalar relativistic BS-DFT calculations were performed on **1** (see Computational Details). The calculated exchange interaction is weakly antiferromagnetic with *J* value of -0.42 cm$^{-1}$, and this is in agreement with the exchange value obtained from the fit (-0.15 cm$^{-1}$). The total magnetic interaction between the Dy(III) centres is -0.008 cm$^{-1}$, indicating the presence of ferromagnetic dipolar interaction (0.142 cm$^{-1}$) between the large moments on Dy(III) ions, and this value is of rather similar strength to the exchange value. This ferromagnetic dipolar interaction originates from the near parallel alignment of local anisotropy axes (see Figure 9). Both exchange and dipolar interactions are competing, and a slightly dominant exchange contribution results in a stabilization of non-magnetic ground state. As a result of antiferromagnetic interaction between the two Dy(III) centres, we noticed that the g$_{zz}$ value of the exchange-coupled ground state approaches to

zero. Moreover, a very small tunnel splitting $\sim 10^{-8}$ cm$^{-1}$ is noticed for the two low-lying doublets (see Table 2 and Figure 11). The significant large tunnel splitting of $3.2 \times 10^{-5}$ via third exchange doublet indicates that magnetic relaxation occurs via this KD. The third exchange doublet is located at $\sim 240$ cm$^{-1}$, which is very close to the observed magnetization blockade of $\sim 239$ cm$^{-1}$ from the single-ion anisotropy studies on individual Dy(III) ions. Therefore, the presence of significant transverse anisotropy, asymmetric CF interactions at mononuclear level, and a very weak Dy···Dy antiferromagnetic interaction clearly explains why complex **1** lacks zero-field SMM behavior.
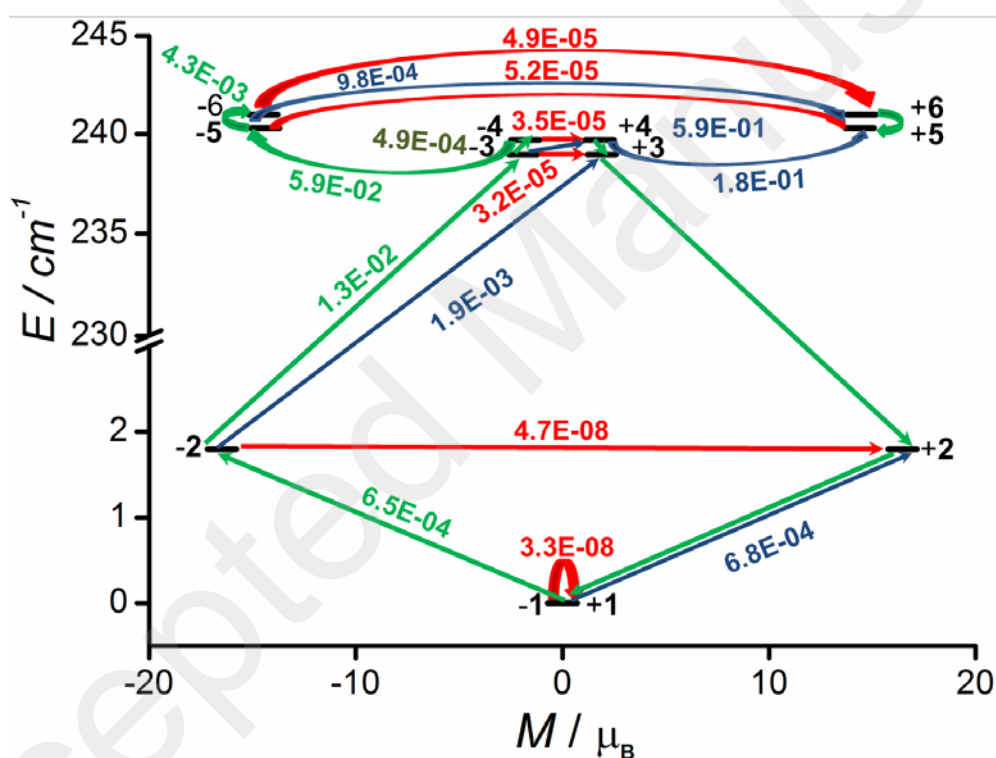


**Figure 11**. Mechanism of magnetic relaxation in the exchange-coupled system in **1**. Red arrows show the possibility of quantum tunnelling of magnetization within each doublets, while the green and blue arrows show the possible relaxation through Raman/Orbach process.

**Conclusion**

We describe a dinuclear Dy(III) complex where both metal centres are present in a PBP geometry. The axial positions are occupied by negatively charged chloride ligands. Theoretical *ab initio* calculations indicate a highly axial ground state for both Dy(III) ions; however, due to the presence of unique intermediate type ligand field in the PBP geometry QTM is not suppressed and restricts the single-ion relaxation to occur via the first excited KD. Thus, despite the presence of significant magnetic anisotropy on individual metal ions, the whole dinuclear system as well as the 10% diluted sample lack zero-field SMM behaviour but show the same in the presence of small *dc* fields. The short Dy---Dy distance and the very strong intermolecular non-covalent interactions generate strong transverse anisotropy. This. along with weak Dy---Dy antiferromagnetic interactions are probably responsible for the zero-field SMM silence of the sample. However, in the presence of a small optimum biased *dc* field both the complexes, **1** and **1$_{10}$** displayed SMM behaviour with $U_{eff}$ = 83(17) K, $\tau_0$= 2(4)×10$^{-12}$ s for **1$_{10}$** at 800 Oe applied field.

## Conflicts of interest

The authors declare no competing financial interest.

## Acknowledgments

## Reference

1. R. Sessoli, D. Gatteschi, A. Caneschi and M. A. Novak, *Nature*, 1993, **365**, 141-143.

2. A. Gaita-Ariño, F. Luis, S. Hill and E. Coronado, *Nat. Chem.*, 2019, **11**, 301-309.

3. A. J. Tasiopoulos, A. Vinslava, W. Wernsdorfer, K. A. Abboud and G. Christou, *Angew. Chem. Int. Ed.*, 2004, **43**, 2117-2121.

4. C. Papatriantafyllopoulou, E. E. Moushi, G. Christou and A. J. Tasiopoulos, *Chem. Soc. Rev.*, 2016, **45**, 1597-1628.

5. A. Escuer, J. Esteban, S. P. Perlepes and T. C. Stamatatos, *Coord. Chem. Rev.*, 2014, **275**, 87-129.

6. T. Shiga, H. Nojiri and H. Oshio, *Inorg. Chem.*, 2020, **59**, 4163-4166.

7. J. Acharya, A. Swain, A. Chakraborty, V. Kumar, P. Kumar, J. F. Gonzalez, O. Cador, F. Pointillart, G. Rajaraman and V. Chandrasekhar, *Inorg. Chem.*, 2019, **58**, 10725-10735.

8. A. Dey, J. Acharya and V. Chandrasekhar, *Chem. Asian J.*, 2019, **14**, 4433-4453.

9. A. Chakraborty, J. Goura, P. Kalita, A. Swain, G. Rajaraman and V. Chandrasekhar, *Dalton Trans.*, 2018, **47**, 8841-8864.

10. D. N. Woodruff, R. E. P. Winpenny and R. A. Layfield, *Chem. Rev.*, 2013, **113**, 5110-5148.

11. Z. Zhu, M. Guo, X.-L. Li and J. Tang, *Coord. Chem. Rev.*, 2019, **378**, 350-364.

12. J. Lu, M. Guo and J. Tang, *Chem. Asian J.*, 2017, **12**, 2772-2779.

13. K. S. Pedersen, M. Sigrist, M. A. Sørensen, A.-L. Barra, T. Weyhermüller, S. Piligkos, C. A. Thuesen, M. G. Vinum, H. Mutka, H. Weihe, R. Clérac and J. Bendix, *Angew. Chem. Int. Ed.*, 2014, **53**, 1351-1354.

14. J. Martínez-Lillo, M. Julve and E. K. Brechin, *Polyhedron*, 2015, **98**, 35-39.

15. X. Feng, J.-L. Liu, K. S. Pedersen, J. Nehrkorn, A. Schnegg, K. Holldack, J. Bendix, M. Sigrist, H. Mutka, D. Samohvalov, D. Aguilà, M.-L. Tong, J. R. Long and R. Clérac, *Chem.Comm.*, 2016, **52**, 12905-12908.

16. S. K. Singh and G. Rajaraman, *Nat. Commun.*, 2016, **7**, 10669.

17. C. H. Woodall, G. A. Craig, A. Prescimone, M. Misek, J. Cano, J. Faus, M. R. Probert, S. Parsons, S. Moggach, J. Martínez-Lillo, M. Murrie, K. V. Kamenev and E. K. Brechin, *Nat. Commun.*, 2016, **7**, 13870.

18. A. H. Pedersen, M. Julve, E. K. Brechin and J. Martínez-Lillo, *CrystEngComm*, 2017, **19**, 503-510.

19. C. Rojas-Dotti, N. Moliner, R. González and J. Martínez-Lillo, *Polyhedron*, 2018, **144**, 82-87.

20. A. Sanchis-Perucho, C. Rojas-Dotti, N. Moliner and J. Martínez-Lillo, *Dalton Trans.*, 2019, **48**, 370-373.

21. S. K. Langley, D. P. Wielechowski, V. Vieru, N. F. Chilton, B. Moubaraki, L. F. Chibotaru and K. S. Murray, *Chem.Comm.*, 2015, **51**, 2044-2047.

22. M. A. Antunes, L. C. J. Pereira, I. C. Santos, M. Mazzanti, J. Marçalo and M. Almeida, *Inorg. Chem.*, 2011, **50**, 9915-9917.

23. J. D. Rinehart and J. R. Long, *J. Am. Chem. Soc.*, 2009, **131**, 12558-12559.

24. J. D. Rinehart, K. R. Meihaus and J. R. Long, *J. Am. Chem. Soc.*, 2010, **132**, 7572-7573.

25. K. R. Meihaus and J. R. Long, *Dalton Trans.*, 2015, **44**, 2517-2528.

26. J. T. Coutinho, M. A. Antunes, L. C. J. Pereira, H. Bolvin, J. Marçalo, M. Mazzanti and M. Almeida, *Dalton Trans.*, 2012, **41**, 13568-13571.

27. J. D. Rinehart and J. R. Long, *Dalton Trans.*, 2012, **41**, 13572-13574.

28.     J. J. Baldoví, S. Cardona-Serra, J. M. Clemente-Juan, E. Coronado and A. Gaita-Ariño, *Chem. Sci.*, 2013, **4**, 938-946.

29.     O. Waldmann, *Inorg. Chem.*, 2007, **46**, 10035-10037.

30.     N. Ishikawa, M. Sugita, T. Ishikawa, S.-y. Koshihara and Y. Kaizu, *J. Am. Chem. Soc.*, 2003, **125**, 8694-8695.

31.     F.-S. Guo, B. M. Day, Y.-C. Chen, M.-L. Tong, A. Mansikkamäki and R. A. Layfield, *Science*, 2018, **362**, 1400-1403.

32.     F.-S. Guo, B. M. Day, Y.-C. Chen, M.-L. Tong, A. Mansikkamäki and R. A. Layfield, *Angew. Chem. Int. Ed.*, 2017, **56**, 11445-11449.

33.     C. A. P. Goodwin, F. Ortu, D. Reta, N. F. Chilton and D. P. Mills, *Nature*, 2017, **548**, 439.

34.     J. D. Rinehart and J. R. Long, *Chem. Sci.*, 2011, **2**, 2078-2085.

35.     L. Ungur and L. F. Chibotaru, *Inorg. Chem.*, 2016, **55**, 10043-10056.

36.     N. F. Chilton, *Inorg. Chem.*, 2015, **54**, 2097-2099.

37.     P. Kalita, J. Acharya and V. Chandrasekhar, *J. Magn. Magn. Mater*, 2020, **498**, 166098.

38.     J. Liu, Y.-C. Chen, J.-L. Liu, V. Vieru, L. Ungur, J.-H. Jia, L. F. Chibotaru, Y. Lan, W. Wernsdorfer, S. Gao, X.-M. Chen and M.-L. Tong, *J. Am. Chem. Soc.*, 2016, **138**, 5441-5450.

39.     Y.-S. Ding, N. F. Chilton, R. E. P. Winpenny and Y.-Z. Zheng, *Angew. Chem. Int. Ed.*, 2016, **55**, 16071-16074.

40.     S. K. Gupta, T. Rajeshkumar, G. Rajaraman and R. Murugavel, *Chem. Sci.*, 2016, **7**, 5181-5191.

41.     P. Evans, D. Reta, C. A. P. Goodwin, F. Ortu, N. F. Chilton and D. P. Mills, *Chem.Comm.*, 2020, **56**, 5677-5680.

42. T. Han, M. J. Giansiracusa, Z.-H. Li, Y.-S. Ding, N. F. Chilton, R. E. P. Winpenny and Y.-Z. Zheng, *Chem. -Eur. J.*, 2020, **26**, 6773-6777.

43. M. He, F.-S. Guo, J. Tang, A. Mansikkamäki and R. A. Layfield, *Chem. Sci.*, 2020, **11**, 5745-5752.

44. S. K. Langley, D. P. Wielechowski, V. Vieru, N. F. Chilton, B. Moubaraki, L. F. Chibotaru and K. S. Murray, *Chem. Sci.*, 2014, **5**, 3246-3256.

45. S. K. Langley, L. Ungur, N. F. Chilton, B. Moubaraki, L. F. Chibotaru and K. S. Murray, *Inorg. Chem.*, 2014, **53**, 4303-4315.

46. S. K. Langley, N. F. Chilton, B. Moubaraki and K. S. Murray, *Inorg. Chem. Front.*, 2015, **2**, 867-875.

47. B. S. Furniss; Hannaford, A. J.; Smith, P. W. G.; Tatchell, A. R., *Vogel's textbook of practical organic chemistry*, 5th ed. edn., **1989**.

48. *Sheldrick, G. M. SADABS: A software for empirical absorption correction, Ver. 2.05*, University of Göttingen, Göttingen, Germany, **2002**.

49. *SHELXTL Reference Manual*, Bruker Analytical X-ray Systems, Inc.: Madison, WI, **2000**.

50. G. Sheldrick, *Acta Crystallogr. A*, 2008, **64**, 112-122.

51. O. V. Dolomanov, L. J. Bourhis, R. J. Gildea, J. A. K. Howard and H. Puschmann, *J. Appl. Crystallogr.*, 2009, **42**, 339-341.

52. K. Bradenburg, *Diamond, Ver. 3.1eM, Crystal Impact GbR*, Bonn, Germany, **2005**.

53. F. Neese, *Wiley Interdiscip. Rev. Comput. Mol. Sci.*, 2018, **8**, e1327.

54. F. Neese, *Wiley Interdiscip. Rev. Comput. Mol. Sci.*, 2012, **2**, 73-78.

55. F. Aquilante, J. Autschbach, R. K. Carlson, L. F. Chibotaru, M. G. Delcey, L. De Vico, I. F. Galvan, N. Ferre, L. M. Frutos, L. Gagliardi, M. Garavelli, A. Giussani, C. E. Hoyer, G. Li Manni, H. Lischka, D. X. Ma, P. A. Malmqvist, T. Muller, A. Nenov,

M. Olivucci, T. B. Pedersen, D. L. Peng, F. Plasser, B. Pritchard, M. Reiher, I. Rivalta, I. Schapiro, J. Segarra-Marti, M. Stenrup, D. G. Truhlar, L. Ungur, A. Valentini, S. Vancoillie, V. Veryazov, V. P. Vysotskiy, O. Weingart, F. Zapata and R. Lindh, *J. Comput. Chem.*, 2016, **37**, 506-541.

56. B. O. Roos, R. Lindh, P. A. Malmqvist, V. Veryazov, P. O. Widmark and A. C. Borin, *J. Phys.Chem. A*, 2008, **112**, 11431-11435.

57. B. O. Roos, V. Veryazov and P. O. Widmark, *Theor. Chem. Acc.*, 2004, **111**, 345-351.

58. P. A. Malmqvist, B. O. Roos and B. Schimmelpfennig, *Chem. Phys. Lett.*, 2002, **357**, 230-240.

59. L. F. Chibotaru and L. Ungur, *J. Chem. Phys.*, 2012, **137**, 064112.

60. K. L. M. Harriman, J. J. Le Roy, L. Ungur, R. J. Holmberg, I. Korobkov and M. Murugesu, *Chem. Sci.*, 2017, **8**, 231-240.

61. P. Zhang, M. Perfetti, M. Kern, P. P. Hallmen, L. Ungur, S. Lenz, M. R. Ringenberg, W. Frey, H. Stoll, G. Rauhut and J. van Slageren, *Chem. Sci.*, 2018, **9**, 1221-1230.

62. I. F. Diaz-Ortega, J. M. Herrera, D. Aravena, E. Ruiz, T. Gupta, G. Rajaraman, H. Nojiri and E. Colacio, *Inorg. Chem.*, 2018, **57**, 6362-6375.

63. I. F. Diaz-Ortega, J. M. Herrera, A. Reyes Carmona, J. R. Galan-Mascaros, S. Dey, H. Nojiri, G. Rajaraman and E. Colacio, *Front. Chem.*, 2018, **6**, 537.

64. H. M. Dong, H. Y. Li, Y. Q. Zhang, E. C. Yang and X. J. Zhao, *Inorg. Chem.*, 2017, **56**, 5611-5622.

65. S. K. Langley, D. P. Wielechowski, V. Vieru, N. F. Chilton, B. Moubaraki, B. F. Abrahams, L. F. Chibotaru and K. S. Murray, *Angew. Chem. Int. Ed.*, 2013, **52**, 12014-12019.

66. H. Tian, L. Ungur, L. Zhao, S. Ding, J. Tang and L. F. Chibotaru, *Chem. -Eur. J.*, 2018, **24**, 9928-9939.

67.  B. A. Hess, *Phys. Rev. A*, 1986, **33**, 3742-3748.

68.  D. A. Pantazis and F. Neese, *J. Chem. Theory Comput.*, 2009, **5**, 2229-2238.

69.  K. Yamaguchi, Y. Takahara and T. Fueno, *Ab-Initio Molecular Orbital Studies of Structure and Reactivity of Transition Metal-OXO Compounds*,1986.

70.  J. Acharya, S. Biswas, J. van Leusen, P. Kumar, V. Kumar, R. S. Narayanan, P. Kögerler and V. Chandrasekhar, *Cryst. Growth Des.*, 2018, **18**, 4004-4016.

71.  S. Das, S. Hossain, A. Dey, S. Biswas, E. Pardo, F. Lloret and V. Chandrasekhar, *Eur. J. Inorg. Chem.*, 2014, **2014**, 3393-3400.

72.  V. Chandrasekhar, S. Das, A. Dey, S. Hossain, F. Lloret and E. Pardo, *Eur. J. Inorg. Chem.*, 2013, **2013**, 4506-4514.

73.  S. Biswas, S. Das, J. van Leusen, P. Kögerler and V. Chandrasekhar, *Eur. J. Inorg. Chem.*, 2014, **2014**, 4159-4167.

74.  S. Biswas, S. Das, J. Acharya, V. Kumar, J. van Leusen, P. Kögerler, J. M. Herrera, E. Colacio and V. Chandrasekhar, *Chem. -Eur. J.*, 2017, **23**, 5154-5170.

75.  I. Hargittai, *Angew. Chem. Int. Ed.*, 1997, **36**, 2525-2525.

76.  H. Zabrodsky, S. Peleg and D. Avnir, *J. Am. Chem. Soc.*, 1992, **114**, 7843-7851.

77.  Z.-F. Yang, Y.-M. Tian, W.-Y. Zhang, P. Chen, H.-F. Li, Y.-Q. Zhang and W.-B. Sun, *Dalton Trans.*, 2019, **48**, 4931-4940.

78.  J. O. Moilanen, A. Mansikkamäki, M. Lahtinen, F.-S. Guo, E. Kalenius, R. A. Layfield and L. F. Chibotaru, *Dalton Trans.*, 2017, **46**, 13582-13589.

79.  O. Kahn, *Molecular magnetism*, VCH, **1993**.

80.  J. K. Ou-Yang, N. Saleh, G. Fernandez Garcia, L. Norel, F. Pointillart, T. Guizouarn, O. Cador, F. Totti, L. Ouahab, J. Crassous and B. Le Guennic, *Chem.Comm.*, 2016, **52**, 14474-14477.

81. P.-E. Car, M. Perfetti, M. Mannini, A. Favre, A. Caneschi and R. Sessoli, *Chem.Comm.*, 2011, **47**, 3751-3753.

82. T. T. da Cunha, J. Jung, M.-E. Boulon, G. Campo, F. Pointillart, C. L. M. Pereira, B. Le Guennic, O. Cador, K. Bernot, F. Pineider, S. Golhen and L. Ouahab, *J. Am. Chem. Soc.*, 2013, **135**, 16332-16335.

83. C. Dekker, A. F. M. Arts, H. W. de Wijn, A. J. van Duyneveldt and J. A. Mydosh, *Phys. Rev. B*, 1989, **40**, 11243-11251.

84. K. S. Cole and R. H. Cole, *J. Chem. Phys.*, 1941, **9**, 341-351.

85. P. T. Z. Jinkui, *Lanthanide Single Molecule Magnets*, Spinger, **2015**.

86. A. Abragam and B. Bleaney, *Electron Paramagnetic Resonance of Transition Ions*, Clarendon Press. Oxford, **1970**.

87. K. N. Shrivastava, *Phys. Status Solidi B*, 1983, **117**, 437-458.

88. A. Singh and K. N. Shrivastava, *Phys. Status Solidi B*, 1979, **95**, 273-277.

89. R. Orbach, *Proc. Phys. Soc.*, 1961, **77**, 821-826.

90. L. Spree, C. Schlesier, A. Kostanyan, R. Westerström, T. Greber, B. Büchner, S. M. Avdoshenko and A. A. Popov, *Chem. -Eur. J.*, 2020, **26**, 2436-2449.

91. C. A. Gaggioli and L. Gagliardi, *Inorg. Chem.*, 2018, **57**, 8098-8105.

92. A. B. Canaj, S. Dey, E. R. Marti, C. Wilson, G. Rajaraman and M. Murrie, *Angew. Chem. Int. Ed.*, 2019, **58**, 14146-14151.

93. S. Dey, G. Velmurugan and G. Rajaraman, *Dalton Trans.*, 2019, **48**, 8976-8988.

94. D. Aravena, M. Atanasov and F. Neese, *Inorg. Chem.*, 2016, **55**, 4457-4469.

95. A. Kerridge, *Computational Methods in Lanthanide and Actinide Chemistry*, 2015, 121-146.

96. S. K. Singh, T. Gupta and G. Rajaraman, *Inorg. Chem.*, 2014, **53**, 10835-10845.

97.     S. K. Singh, T. Gupta, M. Shanmugam and G. Rajaraman, *Chem.Comm.*, 2014, **50**, 15513-15516.

98.     S. K. Singh, B. Pandey, G. Velmurugan and G. Rajaraman, *Dalton Trans*, 2017, **46**, 11913-11924.

99.     L. Ungur and L. F. Chibotaru, *Phys. Chem. Chem. Phys.*, 2011, **13**, 20086-20090.

100.    R. J. Blagg, L. Ungur, F. Tuna, J. Speak, P. Comar, D. Collison, W. Wernsdorfer, E. J. L. McInnes, L. F. Chibotaru and R. E. P. Winpenny, *Nat. Chem.*, 2013, **5**, 673-678.

101.    K. L. M. Harriman, J. L. Brosmer, L. Ungur, P. L. Diaconescu and M. Murugesu, *J. Am. Chem. Soc.*, 2017, **139**, 1420-1423.

102.    J. Xiong, H.-Y. Ding, Y.-S. Meng, C. Gao, X.-J. Zhang, Z.-S. Meng, Y.-Q. Zhang, W. Shi, B.-W. Wang and S. Gao, *Chem. Sci.*, 2017, **8**, 1288-1294.

103.    B. S. Sran, J. F. Gonzalez, V. Montigaud, B. Le Guennic, F. Pointillart, O. Cador and G. Hundal, *Dalton Trans.*, 2019, **48**, 3922-3929.

104.    F. Pointillart, Y. Le Gal, S. Golhen, O. Cador and L. Ouahab, *Chem. -Eur. J.*, 2011, **17**, 10397-10404.

105.    C. Y. Chow, H. Bolvin, V. E. Campbell, R. Guillot, J. W. Kampf, W. Wernsdorfer, F. Gendron, J. Autschbach, V. L. Pecoraro and T. Mallah, *Chem. Sci.*, 2015, **6**, 5087-5087.

106.    X. Yi, K. Bernot, O. Cador, J. Luzon, G. Calvez, C. Daiguebonne and O. Guillou, *Dalton Trans.*, 2013, **42**, 6728-6731.

107.    F. Habib and M. Murugesu, *Chem. Soc. Rev.*, 2013, **42**, 3278-3288.

108.    G. Huang, X. Yi, J. Jung, O. Guillou, O. Cador, F. Pointillart, B. Le Guennic and K. Bernot, *Eur. J. Inorg. Chem.*, 2018, **2018**, 326-332.

109.    E. Moreno-Pineda, G. Taran, W. Wernsdorfer and M. Ruben, *Chem. Sci.*, 2019, **10**, 5138-5145.

110. J. Flores Gonzalez, F. Pointillart and O. Cador, *Inorg. Chem. Front.*, 2019, **6**, 1081-1086.

111. L. Escalera-Moreno, J. J. Baldoví, A. Gaita-Ariño and E. Coronado, *Chem. Sci.*, 2020, **11**, 1593-1598.

112. F. Ortu, D. Reta, Y.-S. Ding, C. A. P. Goodwin, M. P. Gregson, E. J. L. McInnes, R. E. P. Winpenny, Y.-Z. Zheng, S. T. Liddle, D. P. Mills and N. F. Chilton, *Dalton Trans.*, 2019, **48**, 8541-8545.

113. M.-E. Boulon, G. Cucinotta, J. Luzon, C. Degl'Innocenti, M. Perfetti, K. Bernot, G. Calvez, A. Caneschi and R. Sessoli, *Angew. Chem. Int. Ed.*, 2013, **52**, 350-354.

114. J. Liu, Y. C. Chen, J. L. Liu, V. Vieru, L. Ungur, J. H. Jia, L. F. Chibotaru, Y. Lan, W. Wernsdorfer, S. Gao, X. M. Chen and M. L. Tong, *J. Am. Chem.. Soc*, 2016, **138**, 5441-5450.

115. Y. C. Chen, J. L. Liu, L. Ungur, J. Liu, Q. W. Li, L. F. Wang, Z. P. Ni, L. F. Chibotaru, X. M. Chen and M. L. Tong, *J. Am. Chem. Soc.*, 2016, **138**, 2829-2837.

116. L. Gagliardi, R. Lindh and G. Karlstrom, *J. Chem. Phys.*, 2004, **121**, 4494-4500.

117. D. Aravena and E. Ruiz, *Inorg. Chem.*, 2013, **52**, 13770-13778.

# Slow Magnetic Relaxation in a Homo Dinuclear Dy(III) Complex in a Pentagonal Bipyamidal Geometry

*Joydev Acharya,[a] Naushad Ahmed,[#b] Jessica Flores Gonzalez,[#c] Pawan Kumar,[a] Olivier Cador,[c] Saurabh Kumar Singh,\*[d] Fabrice Pointillart,\*[c] Vadapalli Chandrasekhar\*[a,b]*
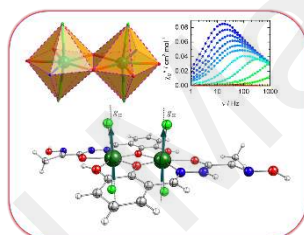
A homodinuclear complex of Dy(III) has been synthesized and characterised. Magnetic analysis disclosed the field induced slow magnetic relaxation of the complex.